Comparing the tsunamigenic potential of two alternative earthquake rupture scenarios in the Ionian Sea

Authors	ORCID	e-mail
Basili, Roberto	0000-0002-1213-0828	roberto.basili@ingv.it
Volpe, Manuela	0000-0003-4551-3339	manuela.volpe@ingv.it
Maesano, Francesco Emanuele	0000-0002-5652-1548	francesco.maesano@ingv.it
Tiberti, Mara Monica	0000-0003-2504-853X	mara.tiberti@ingv.it

Istituto Nazionale di Geofisica e Vulcanologia

Via di Vigna Murata, 605 - 00143 Roma, Italy

Reviewed by Stefano Lorito.

Available online: 18 December 2020.

Basili R., Volpe M., Maesano F.M., Tiberti M.M. (2020). Comparing the tsunamigenic potential of two alternative earthquake rupture scenarios in the Ionian Sea. INGV internal report, DOI: 10.5281/zenodo.4353092.

Executive summary

The Alfeo Fault System (AFS; Figure 1) was recently proposed to be the actual lateral termination of the Calabrian Arc slab (Gutscher et al., 2017; Maesano et al., 2017, 2020). The AFS was previously identified by high-resolution seismic surveys by Polonia et al. (2011, 2016), Gallais et al. (2013), and Gutscher et al. (2016), who characterized with great detail its shallow structural features. Then, Maesano et al. (2020) explored and characterized the deep-seated portion of the AFS and concluded that it represents the major lithospheric tear in the area and that it is mechanically decoupled from the AFS shallow features.

The Ionian Sea is a region that was affected by several local earthquakes and tsunamis in the past (Maramai et al., 2014; Guidoboni et al., 2019; Rovida et al., 2019, 2020). Several potential crustal fault sources and the Calabrian subduction interface contributing to the tsunami hazard in the region have already been investigated (Basili et al., 2013, 2019; Selva et al., 2016; Scala et al., 2020; Tonini et al., 2020) and we question now whether the deep-seated AFS could represent an additional potential source for earthquake-generated tsunamis in the region. The purpose of this study is to verify through numerical tsunami simulations if a hypothetical earthquake rupture on the AFS could generate a significant tsunami.

As a term of comparison for our analysis, we adopt the tsunami modeled by Argnani et al. (2012), which is one of the latest attempts at identifying the source of the 1693 tsunami, a task that is also being tackled by many other authors (Piatanesi and Tinti, 1998; Tinti et al., 2001; Gutscher et al., 2006; Pirrotta and Barbano, 2020). To this end, we model an earthquake rupture of the same moment magnitude and, likewise, use a homogeneous slip distribution.

The results of the simulations presented in this report confirm that a hypothetical earthquake rupture on the AFS can produce a tsunami with wave amplitudes in the same order of magnitude as that of the tsunami simulated by Argnani et al. (2012) at several sites on the coastlines of the Ionian Sea.

Important notice: the analysis presented here is not intended to reproduce the 1693 tsunami nor to propose the AFS as a candidate source for that earthquake and/or tsunami.

Fault sources and earthquake ruptures

The fault sources in this analysis are shown in Figure 1, and the parameters of the earthquake ruptures are reported in Table 1. We adopt planar rectangular earthquake sources with the seismic parameters set by Argnani et al. (2012). Length, width, slip, and rake are all the same, whereas the main differences between the two earthquake rupture sources are their location, strike, dip, and depth. The small strike deviations introduced in the Argnani et al. (2012) model are not considered here. The seafloor displacement, which is the first input to the tsunami simulation, is approximated as the results of an instantaneous rupture. Figure 2 shows a profile oriented SW-NE for easy comparison of the effect on the displacement due to the dip and depth differences of the two ruptures. The displacement profile is sampled on a line through the rupture center and orthogonal to its strike, then projected onto the topographic profile. The combined effect of dip and depth induced significant footwall uplift in the ALF and combined hanging wall subsidence and uplift in the MEF.

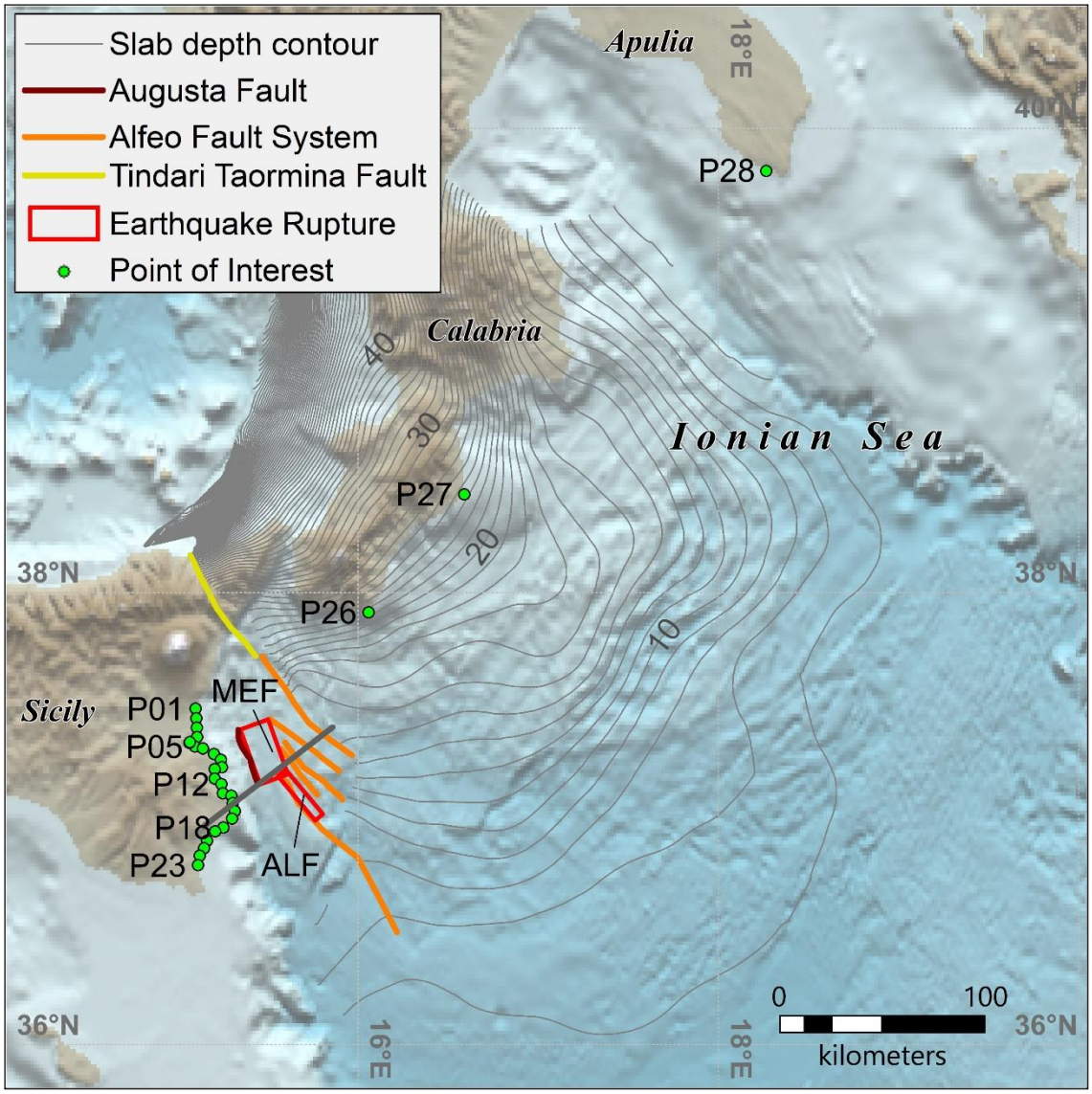

Figure 1. Map of the study area showing the Calabrian slab contours (interval 1 km, max 100 km) (Maesano et al., 2017), the Alfeo Fault System and Tindari-Taormina Fault (Maesano et al., 2020), the Augusta Fault (Argnani et al., 2012), and the location of the points of interest where tsunami time histories have been saved. Earthquake rupture parameters are listed in Table 1. The profile (SW-NE grey line across faults) is shown in Figure 2)

Table 1. Parameters of the two earthquake rupture scenarios. Longitude, latitude, and depth (columns Lon C, Lat C, Depth C) are the position of the earthquake rupture center.

ID	Lon C (°)	Lat C (°)	Depth C (km)	L (km)	W (km)	Strike (°)	Dip (°)	Rake (°)	Slip (m)
MEF	15.401	37.279	6.9	28.5	16.5	340	28	270	5
ALF	15.659	37.096	13.9	28.5	16.5	320	72.5	270	5

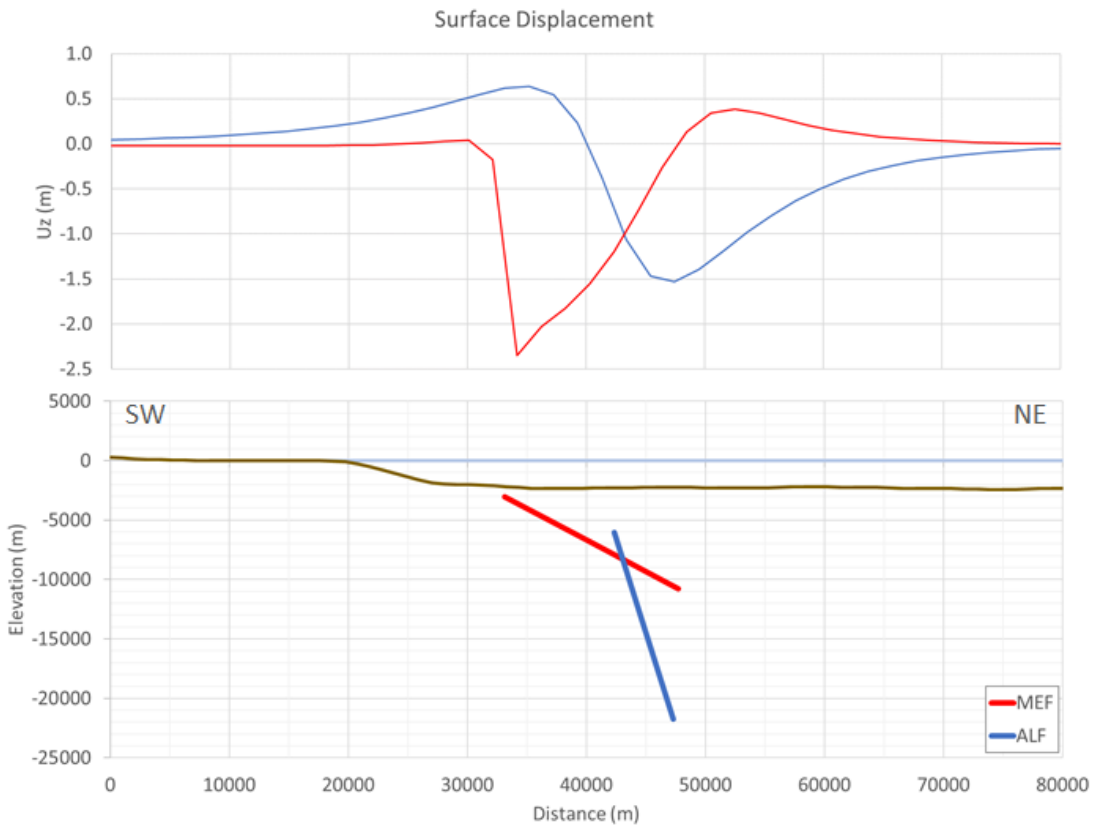

Figure 2. SW-NE profile, from southern Sicily into the Ionian offshore (see Figure 1 for location), crossing almost orthogonally the two earthquake ruptures (bottom). The seafloor (local surface) displacement in the middle of each earthquake rupture is projected onto the profile (top) for comparing the differences that, in this view, depend on dip and depth of the earthquake rupture, being all other parameters equal.

Tsunami scenarios

The numerical tsunami propagation simulations were done using the Tsunami-HySEA, a nonlinear hydrostatic shallow-water multi-GPU code based on a finite-volume method (de la Asunción et al., 2013; Macías et al., 2017), on a 30 arc-sec topo-bathymetric model (Becker et al., 2009). The initial sea-level elevation was obtained by modeling the elastic dislocation on rectangular faults using Okada's code (Okada, 1985). A Kajiura-like filter for the sea bottom–water surface transfer of the dislocation was also applied (Kajiura, 1963), using an average water depth value of 2.5 km. The simulation length was fixed at 2 hours, and time series of the tsunami wave amplitude were stored each 30 sec on a set of points along the coastline of eastern Sicily (see Figure 1).

Figure 3 shows the maximum wave height for the two tsunami scenarios in a portion of the simulation domain, whereas Figure 4 shows the maximum and minimum tsunami amplitudes, retrieved from time series, at the selected points of interest (see Figure 1 for location). The tsunami time series at selected locations in the near-field and far-field are shown in Figure 5 and Figure 6, respectively.

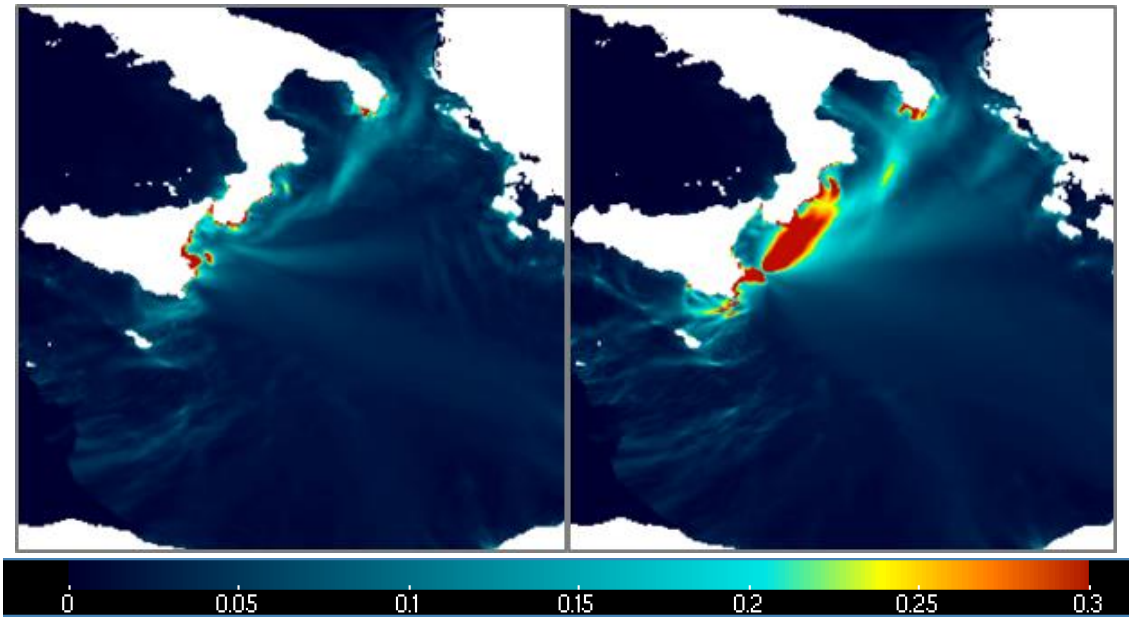

Figure 3. Map of the maximum wave height (m) for the two tsunami scenarios. MEF (left), ALF (right).

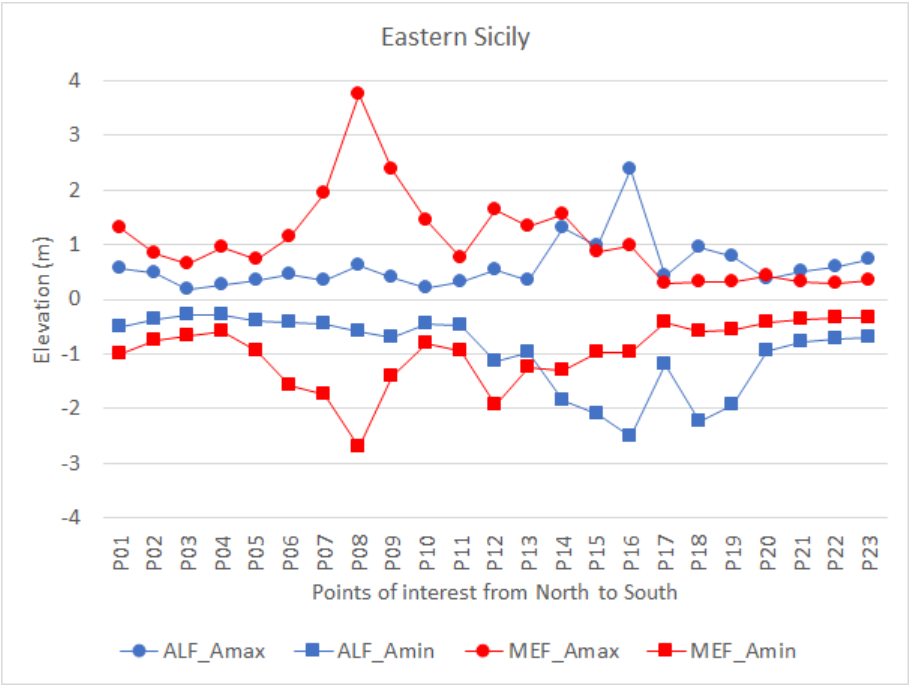

Figure 4. Maximum (Amax) and minimum (Amin) wave amplitudes calculated for the two earthquake rupture scenarios on the coastline of eastern Sicily. The location of the points of interest is shown in Figure 1.

The two tsunami scenarios yield comparable wave amplitudes both in the near- and the far-field of the source, with slightly higher peaks for the MEF source in the near-field. The main noticeable difference between the two scenarios is the opposite polarity of the first wave arrival. This difference can clearly be attributed to the effect of the MEF and ALF different dip angles that determine different subsidence and uplift patterns (Figure 2).

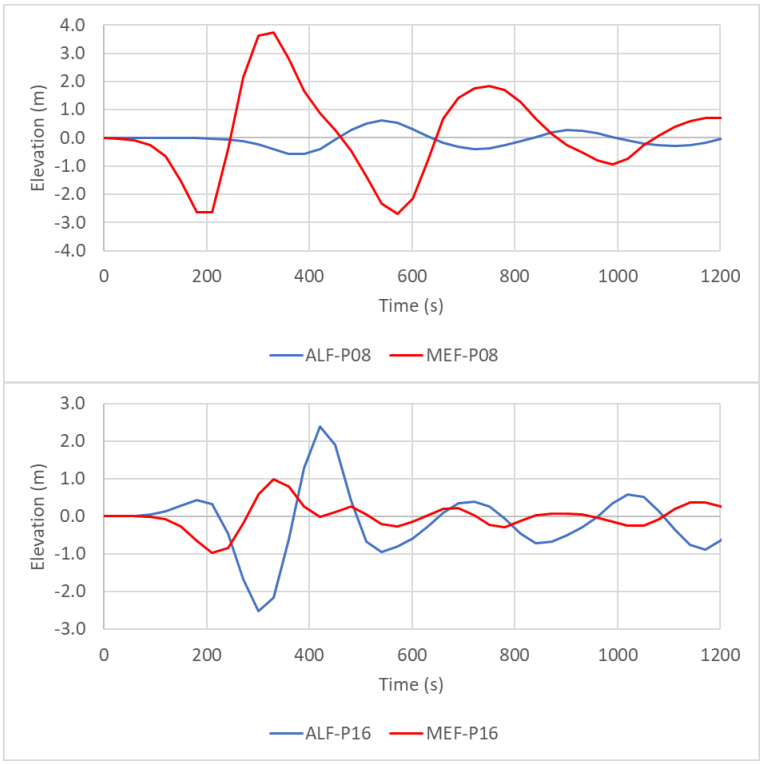

Figure 5. Mareograms recorded at two selected POIs (P08 and P16) on the coast of eastern Sicily (see Figure 1 for location) for the two earthquake rupture scenarios.

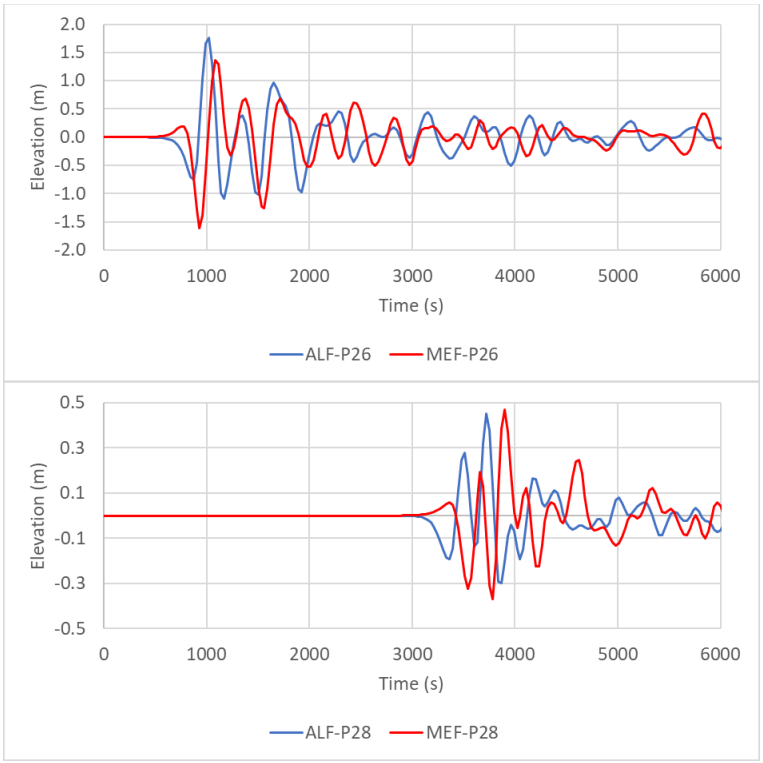

Figure 6. Mareograms recorded at two selected POIs (P26 and P28) on the coast of Calabria (top) and Puglia (bottom) (see Figure 1 for location) for the two earthquake rupture scenarios.

References

Argnani, A., Armigliato, A., Pagnoni, G., Zaniboni, F., Tinti, S., and Bonazzi, C. (2012). Active tectonics along the submarine slope of south-eastern Sicily and the source of the 11 January 1693 earthquake and tsunami. *Nat. Hazards Earth Syst. Sci.* 12, 1311–1319. doi:10.5194/nhess-12-1311-2012.

Basili, R., Brizuela, B., Herrero, A., Iqbal, S., Lorito, S., Maesano, F. E., et al. (2019). NEAMTHM18 Documentation: the making of the TSUMAPS-NEAM Tsunami Hazard Model 2018. Roma, Italy: Istituto Nazionale di Geofisica e Vulcanologia (INGV); DOI: http://doi.org/10.5281/zenodo.3406625.

Basili, R., Tiberti, M. M., Kastelic, V., Romano, F., Piatanesi, A., Selva, J., et al. (2013). Integrating geologic fault data into tsunami hazard studies. *Nat. Hazards Earth Syst. Sci.* 13, 1025–1050. doi:10.5194/nhess-13-1025-2013.

Becker, J. J., Sandwell, D. T., Smith, W. H. F., Braud, J., Binder, B., Depner, J., et al. (2009). Global Bathymetry and Elevation Data at 30 Arc Seconds Resolution: SRTM30_PLUS. *Mar. Geod.* 32, 355–371. doi:10.1080/01490410903297766.

de la Asunción, M., Castro, M. J., Fernández-Nieto, E. D., Mantas, J. M., Acosta, S. O., and González-Vida, J. M. (2013). Efficient GPU implementation of a two waves TVD-WAF method for the two-dimensional one layer shallow water system on structured meshes. *Comput. Fluids* 80, 441–452. doi:10.1016/j.compfluid.2012.01.012.

Gallais, F., Graindorge, D., Gutscher, M.-A., and Klaeschen, D. (2013). Propagation of a lithospheric tear fault (STEP) through the western boundary of the Calabrian accretionary wedge offshore eastern Sicily (Southern Italy). *Tectonophysics* 602, 141–152. doi:10.1016/j.tecto.2012.12.026.

Guidoboni, E., Ferrari, G., Tarabusi, G., Sgattoni, G., Comastri, A., Mariotti, D., et al. (2019). CFTI5Med, the new release of the catalogue of strong earthquakes in Italy and in the Mediterranean area. *Sci. Data* 6, 80. doi:10.1038/s41597-019-0091-9.

Gutscher, M.-A., Dominguez, S., de Lepinay, B. M., Pinheiro, L., Gallais, F., Babonneau, N., et al. (2016). Tectonic expression of an active slab tear from high-resolution seismic and bathymetric data offshore Sicily (Ionian Sea). *Tectonics* 35, 39–54. doi:10.1002/2015TC003898.

Gutscher, M.-A., Kopp, H., Krastel, S., Bohrmann, G., Garlan, T., Zaragosi, S., et al. (2017). Active tectonics of the Calabrian subduction revealed by new multi-beam bathymetric data and high-resolution seismic profiles in the Ionian Sea (Central Mediterranean). *Earth Planet. Sci. Lett.* 461, 61–72. doi:10.1016/j.epsl.2016.12.020.

Gutscher, M.-A., Roger, J., Baptista, M.-A., Miranda, J. M., and Tinti, S. (2006). Source of the 1693 Catania earthquake and tsunami (southern Italy): New evidence from tsunami modeling of a locked subduction fault plane. *Geophys. Res. Lett.* 33, L08309. doi:10.1029/2005GL025442.

Kajiura, K. (1963). The leading wave of a tsunami. *Bull Earthq Res Inst* 41, 535–571.

Macías, J., Castro, M. J., Ortega, S., Escalante, C., and González-Vida, J. M. (2017). Performance Benchmarking of Tsunami-HySEA Model for NTHMP's Inundation Mapping Activities. *Pure Appl. Geophys.* 174, 3147–3183. doi:10.1007/s00024-017-1583-1.

Maesano, F. E., Tiberti, M. M., and Basili, R. (2017). The Calabrian Arc: three-dimensional modelling of the subduction interface. *Sci. Rep.* 7, 8887. doi:10.1038/s41598-017-09074-8.

Maesano, F. E., Tiberti, M. M., and Basili, R. (2020). Deformation and Fault Propagation at the Lateral Termination of a Subduction Zone: The Alfeo Fault System in the Calabrian Arc, Southern Italy. *Front. Earth Sci.* 8. doi:10.3389/feart.2020.00107.

Maramai, A., Brizuela, B., and Graziani, L. (2014). The Euro-Mediterranean Tsunami Catalogue. *Ann. Geophys.* 57. doi:10.4401/ag-6437.

Okada, Y. (1985). Surface deformation due to shear and tensile faults in a half-space. *Bull. Seismol. Soc. Am.* 75, 1135–1154.

Piatanesi, A., and Tinti, S. (1998). A revision of the 1693 eastern Sicily earthquake and tsunami. *J. Geophys. Res. Solid Earth* 103, 2749–2758. doi:10.1029/97JB03403.

Pirrotta, C., and Barbano, M. S. (2020). New Macroseismic and Morphotectonic Constraints to Infer a

Fault Model for the 9 (Mw6.1) and 11 January (Mw7.3) 1693 Earthquakes (Southeastern Sicily). *Front. Earth Sci.* 8, 550851. doi:10.3389/feart.2020.550851.

Polonia, A., Torelli, L., Artoni, A., Carlini, M., Faccenna, C., Ferranti, L., et al. (2016). The Ionian and Alfeo–Etna fault zones: New segments of an evolving plate boundary in the central Mediterranean Sea? *Tectonophysics* 675, 69–90. doi:10.1016/j.tecto.2016.03.016.

Polonia, A., Torelli, L., Mussoni, P., Gasperini, L., Artoni, A., and Klaeschen, D. (2011). The Calabrian Arc subduction complex in the Ionian Sea: Regional architecture, active deformation, and seismic hazard. *Tectonics* 30, n/a-n/a. doi:10.1029/2010TC002821.

Rovida, A., Locati, M., Camassi, R., Lolli, B., and Gasperini, P. (2019). Catalogo Parametrico dei Terremoti Italiani (CPTI15), versione 2.0. 4760 earthquakes. doi:10.13127/CPTI/CPTI15.2.

Rovida, A., Locati, M., Camassi, R., Lolli, B., and Gasperini, P. (2020). The Italian earthquake catalogue CPTI15. *Bull. Earthq. Eng.* 18, 2953–2984. doi:10.1007/s10518-020-00818-y.

Scala, A., Lorito, S., Romano, F., Murphy, S., Selva, J., Basili, R., et al. (2020). Effect of Shallow Slip Amplification Uncertainty on Probabilistic Tsunami Hazard Analysis in Subduction Zones: Use of Long-Term Balanced Stochastic Slip Models. *Pure Appl. Geophys.* 177, 1497–1520. doi:10.1007/s00024-019-02260-x.

Selva, J., Tonini, R., Molinari, I., Tiberti, M. M., Romano, F., Grezio, A., et al. (2016). Quantification of source uncertainties in Seismic Probabilistic Tsunami Hazard Analysis (SPTHA). *Geophys. J. Int.* 205, 1780–1803. doi:10.1093/gji/ggw107.

Tinti, S., Armigliato, A., and Bortolucci, E. (2001). Contribution of tsunami data analysis to constrain the seismic source: the case of the 1693 eastern Sicily earthquake. *J. Seismol.* 5, 41–61. doi:10.1023/A:1009817601760.

Tonini, R., Basili, R., Maesano, F. E., Tiberti, M. M., Lorito, S., Romano, F., et al. (2020). Importance of earthquake rupture geometry on tsunami modelling: the Calabrian Arc subduction interface (Italy) case study. *Geophys. J. Int.* 223, 1805–1819. doi:10.1093/gji/ggaa409.